J. Pharm. Pharmacol. 1990, 42: 606-610
Received March 26, 1990

Effect of Surface Characteristics of Theophylline Anhydrate Powder on Hygroscopic Stability

MAKOTO OTSUKA†, NOBUYOSHI KANENIWA, KATSUMI KAWAKAMI* AND OSAMU UMEZAWA*

School of Pharmaceutical Sciences, Showa University and Department of Pharmacy, Showa University Hospital, Hatanodai 1-5-8, Shinagawa-ku, Tokyo 142, Japan*

Abstract—The hygroscopicity of theophylline anhydrate has been investigated by gas adsorption and hydration kinetic methods. Type I theophylline anhydrate was obtained by recrystallization from distilled water at 95°C, and type II was obtained by dehydration of theophylline monohydrate. The X-ray diffraction pattern of types I and II agreed with the data of theophylline anhydrate. However, the diffraction peaks of the (200) and (400) planes of type I were much stronger than those of type II. The particles of type I were clear crystalline-like single crystals. However, the particles of type II had many cracks. The gas affinity balance (H/N) of type II, measured by gas adsorption, was about 7 times that of type I. After the hygroscopicity of types I and II had been tested at various levels of relative humidity (RH) at 35°C, type I was stable at less than 82% RH, but transformed into the monohydrate at more than 88% RH. Type II was stable at less than 66% RH and transformed into the monohydrate at less than 75% RH. The hydration data of type I at 88% RH and type II at 75% RH were calculated for hydration kinetics using various solid-state kinetic models, but no particular model could be preferred from these data.

Changes in the physicochemical properties of bulk powders may affect their bioavailability through effects on the dissolution rate and this is so with theophylline. Shefter & Higuchi (1963) found that the anhydrate of theophylline was more soluble than the monohydrate. Sutor (1958) and Naqvi & Bhattacharyya (1981), using single crystal X-ray diffraction analysis, reported on the crystal structure of theophylline monohydrate and anhydrate. We described the dehydration kinetics of various dose forms of theophylline monohydrate (Otsuka & Kaneniwa 1988) and concluded that crystal shape and porosity affected the dehydration kinetics of theophylline powders and tablets. The Pharmacopoeia Japonica XI (1986) specifies the anhydrate crystalline form of theophylline. In general, the crystalline form of an organic compound is dependent on the recrystallization solvent. In practice, an organic solvent is not useful because it is difficult to remove it from the bulk powder drug, therefore, the only recrystallization solvents considered safe for formulation are water and ethanol. Shefter & Higuchi (1963) suggested that theophylline anhydrate is crystallized from water above the transition temperature, because this is the stable form above that temperature. There are thus two methods for preparation of the anhydrate from aqueous solution. One (type I) is recrystallization above the transition temperature, and the other (type II) is desorption from theophylline monohydrate by heating. In the present study we have investigated the effects of solid surface characteristics on the hygroscopicity of theophylline anhydrates (types I and II) and their physicochemical stability at high humidity.

Materials and Methods

Materials

Theophylline (Pharmacopoeia Japonica XI) was dissolved in distilled water at 90°C, and the undissolved material was removed by filtration. Saturated theophylline solution was evaporated to dryness under atmospheric pressure at 95°C for 24 h to obtain the type I theophylline anhydrate. Saturated theophylline solution at 90°C was cooled to about 20°C, and the monohydrate crystals were collected by filtration. Type II theophylline anhydrate was then obtained by drying at 100°C for 24 h. Sample powders were sieved with a No. 42 mesh screen (350 μm).

Measurement of specific surface area and particle diameter

The specific surface area was measured by the air permeability method (Type SS-100, Shimadzu Seisakusho Co. Ltd), and the BET gas adsorption method (P700, Shibata Kagaku Ind. Co. Ltd). The average particle diameters (D) of the sample powder were calculated from equation 1 and the data of the specific surface area by assuming sphere and columnar crystal shape (width : length : height = 1 : 1 : 5).

$$D = k/(d\ Sw) \quad (1)$$

where k is a specific shape factor (sphere = 6, columnar = 14), d is powder density and Sw is specific surface area. The specific surface area and average particle diameter of theophylline anhydrate are given in Table 2.

Measurement of powder density

The powder density was measured by using an air pycnometer (Model 930, Beckman Co. Ltd). The sample density was measured three times.

Gas adsorption measurement

The volume of adsorbed nitrogen gas on the sample surface was measured by the BET gas adsorption method (P700, Shibata Kagaku Ind. Co. Ltd). The water adsorbed on the sample surface was measured with a water vapour adsorption instrument (P850, Shibata Kagaku Ind. Co. Ltd). The amount of water adsorbed at 35°C was measured from the length of a quartz spring at 27·8 mm Hg partial water vapour

† Present address and correspondence: M. Otsuka, Dept of Pharmaceutical Technology, Kobe Women's College of Pharmacy, Motoyama-Kitamachi 4-19-1, Higashi-Nada, Kobe-shi 658, Japan.

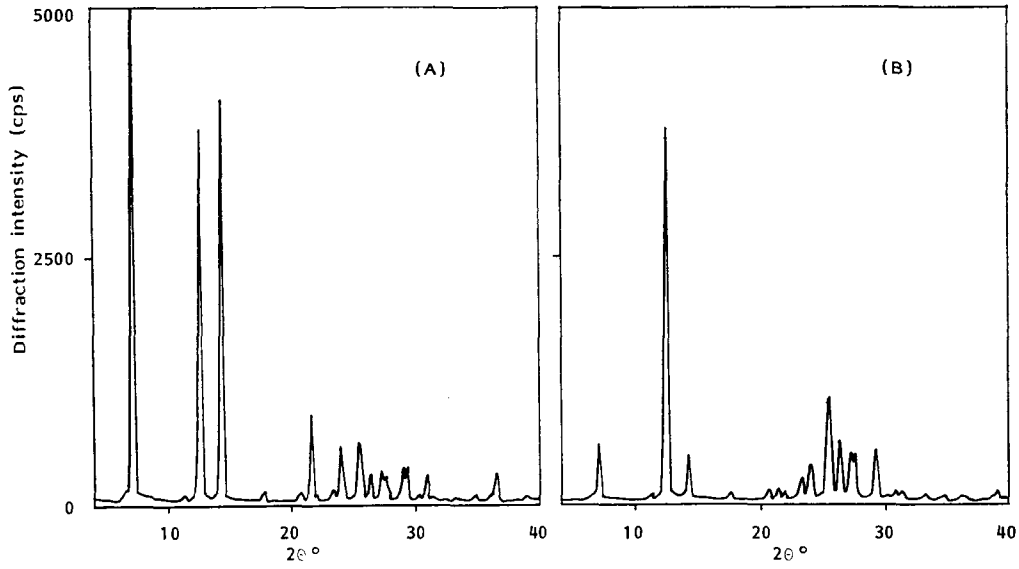

FIG. 1. X-ray diffraction profiles of types I and II theophylline anhydrate. (A), type I; (B), type II.

pressure, in a round flask containing a $NaNO_2$ saturated solution (66% RH at 35°C).

Powder X-ray diffraction analysis

Powder X-ray diffraction was measured at room temperature with a type JDX 7E diffractometer (Nihon Denshi Co. Ltd). The measurement conditions were: target, Cu; filter, Ni; voltage, 30 kV; current, 10 mA; time constant, 2 s; measured from $2\theta = 3°$ to $2\theta = 40°$. The powder was loaded gently into a sample glass holder without orientation of crystals. The intensities of diffraction peaks were reproducible on repeated runs.

Measurement of infrared (IR) spectra

The IR spectra were measured as mulls in Nujol with an IR-2 spectrophotometer (Nihon Bunko Co. Ltd).

Thermal analysis

Differential thermal analysis (DTA) curves were measured with a type DT-20 DTA instrument (Shimadzu Seisakusho Co. Ltd). The heat of fusion was measured by differential scanning calorimetry (DSC) (SC-20B; Shimadzu Seisakusho Co. Ltd). The measurement conditions were: sample weight, 3 mg for DTA and 5 mg for DSC; heating rate, 10°C min^{-1}; N_2 gas flow, 30 mL min^{-1}; sample cell, aluminium crimp cell.

Measurement of water content

Samples (300 mg) were stored over saturated salt solutions at various RH values in desiccators (0 to 95% RH) at 35 ± 1°C, and the water content was determined by weighing.

Results

Characterization of types I and II theophylline anhydrate

Fig. 1 shows the X-ray diffraction profiles of types I and II theophylline anhydrate. The X-ray diffraction pattern and the main diffraction angles of types I and II agreed with the data of theophylline anhydrate in a previous study (Shefter et al 1973; Naqvi & Bhattacharyya 1981) as shown in Table 1. However, the intensities of the (200) and (400) planes of type I were much stronger than those of type II.

Table 1. Intensities of diffraction peaks in X-ray diffraction patterns of theophylline anhydrates.

		Peak intensity (cps)	
2θ (°)	(hkl)[a]	Type I	Type II
7·2	(200)	6055 ± 250	20 ± 5
12·7	(201)	3785 ± 150	3445 ± 220
14·4	(400)	4090 ± 440	560 ± 125
21·7	(202)	896 ± 95	171 ± 33
24·2	(210)	582 ± 65	450 ± 56
25·6	(310)	608 ± 52	932 ± 102
26·6	(211)	291 ± 23	552 ± 60

[a] reflecting plane indices.

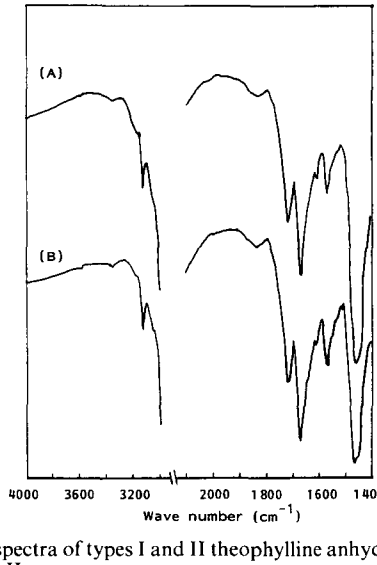

FIG. 2. IR spectra of types I and II theophylline anhydrate. (A), type I; (B), type II.

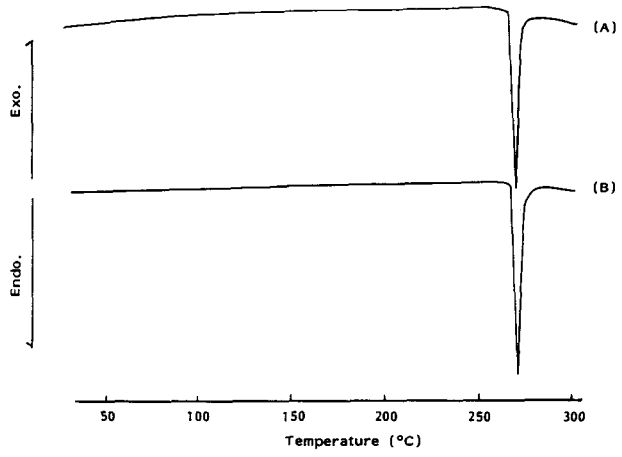

FIG. 3. DTA curves of types I and II theophylline anhydrate.(A), type I; (B), type II.

The IR spectra and the DTA curves of types I and II are shown in Figs 2 and 3. The main absorption peaks were similar. The DTA curves showed endothermic peaks at 266°C for type I and at 267°C for type II. The heats of fusion of types I and II were $27{\cdot}19 \pm 0{\cdot}25$ kJ mol^{-1} and $26{\cdot}90 \pm 0{\cdot}51$ kJ mol^{-1}, respectively.

Fig. 4 shows photomicrographs of typical large crystals of types I and II theophylline anhydrates. The crystalline particles of type I were columnar single crystals. However, the crystals of type II had many cracks. It seems that the secondary particles were formed from fine primary particles.

Table 2 shows the physicochemical properties of theophylline anhydrates. The average particle diameter (Da) measured by the air permeability method of type II was larger than that of type I. However, the average particle diameter (Dg) of type II measured by the BET gas adsorption method was smaller than that of type I. The density of type II ($1{\cdot}499 \pm 0{\cdot}004$ g cm^{-3}) was not significantly different from that of type I ($1{\cdot}513 \pm 0{\cdot}031$ g cm^{-3}). The nitrogen gas adsorption of type I was about 2·5 times that of type II, whereas the gas affinity balance (H/N) of type II was about 7 times that of type I.

Hygroscopicity of types I and II theophylline anhydrates

Fig. 5 shows the water absorption profiles of types I and II at various levels of relative humidity (RH) at 35°C. Type I transformed into the monohydrate at RH higher than 88%, and type II transformed into the monohydrate even at 75% RH. After the hygroscopicity test, the X-ray diffraction profiles of types I and II, in which the water contents increased about 10%, showed typical diffraction profiles of theophylline monohydrate.

The water content versus RH at equilibrium is shown in Fig. 6. Type I was transformed into the monohydrate at RH $>66\%$ whereas, type II was transformed at RH $>82\%$.

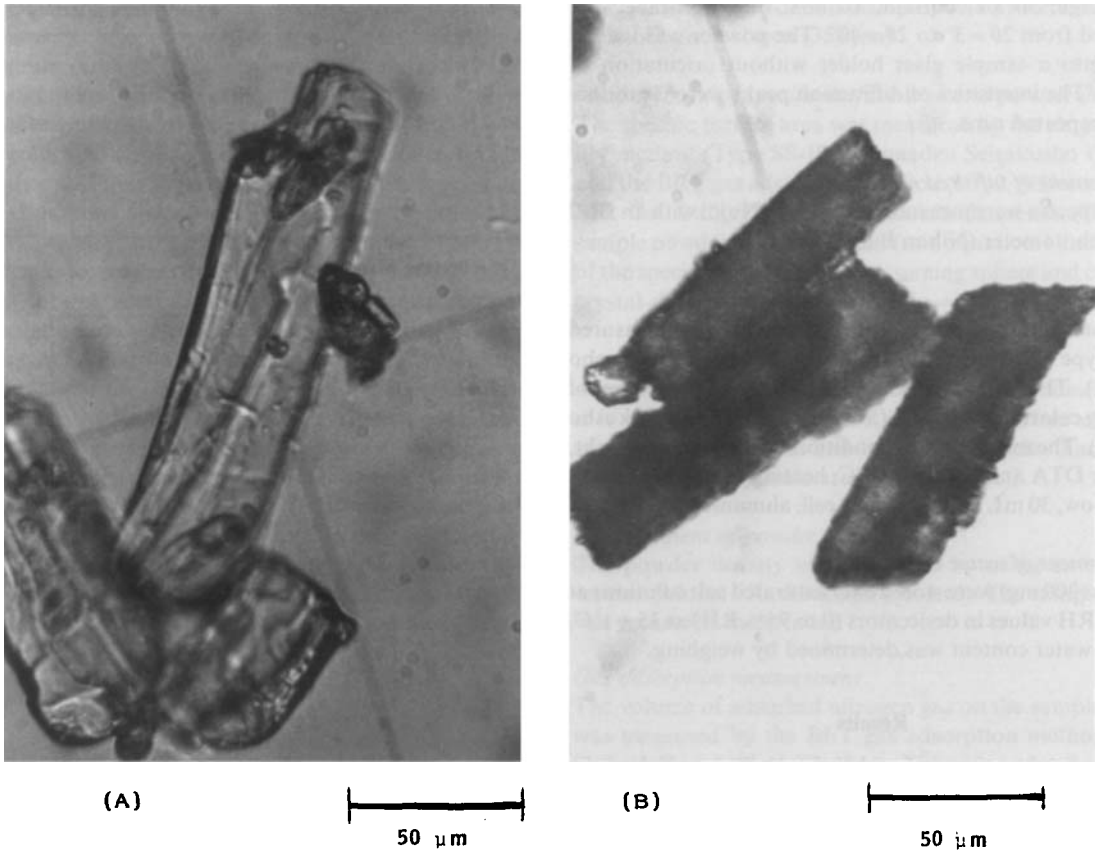

FIG. 4. Photomicrographs of types I and II theophylline anhydrate. (A), type I; (B), type II.

Table 2. Specific surface area ($cm^2\ g^{-1}$), particle diameter (μm) and gas affinity balance (H/N) of theophylline anhydrates.

	Air permeability method		BET gas adsorption method				
Sample	($cm^2\ g^{-1}$)	(μm)	($cm^2\ g^{-1}$)	(μm)	N_2 gas[a] ($mL\ g^{-1}$)	H_2O[b] ($mg\ g^{-1}$)	H/N[c]
Type I	3304 ± 13[d]	$28{\cdot}0^{e} \pm 0{\cdot}2^{d}$ ($12{\cdot}0^{f} \pm 0{\cdot}1$)	1058	$87{\cdot}5^{e}$ ($37{\cdot}5^{f}$)	7·383	4·807	0·5209
Type II	1954 ± 48	$47{\cdot}8^{e} \pm 1{\cdot}1$ ($20{\cdot}4^{f} \pm 0{\cdot}5$)	4993	$18{\cdot}7^{e}$ ($8{\cdot}0^{f}$)	2·874	9·855	3·429

[a] at $P/P_o = 0{\cdot}900$; [b] at 66% RH ($NaNO_2$ saturated suspension) at 35°C; [c] weight ratio of water vapour and nitrogen gas; [d] standard deviation ($n = 3$); [e] assuming columnar crystal shape (width: length: height = 1:1:5); [f] assuming sphere.

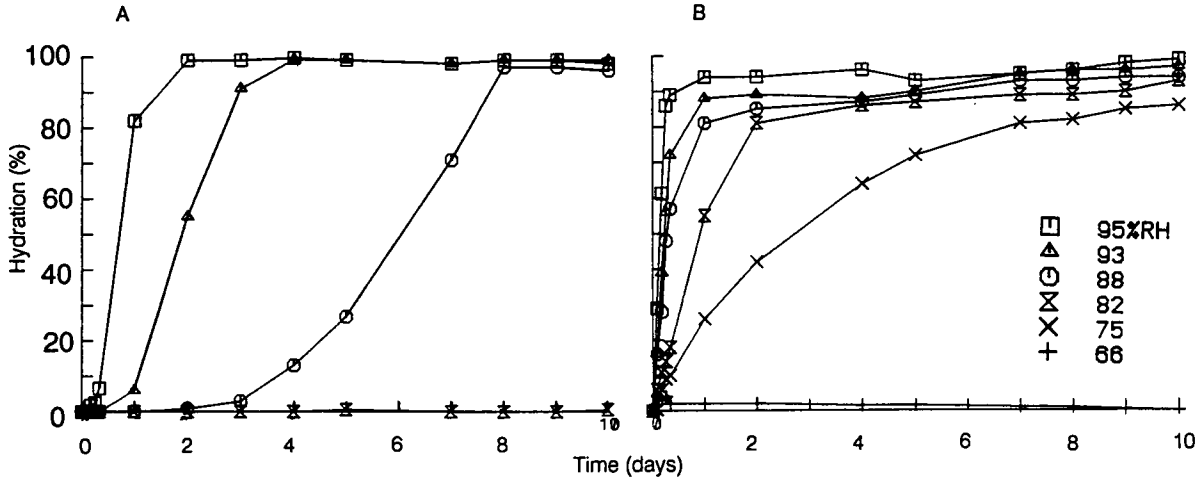

FIG. 5. Hygroscopicity profiles of types I and II theophylline anhydrate. (A), type I; (B), type II.

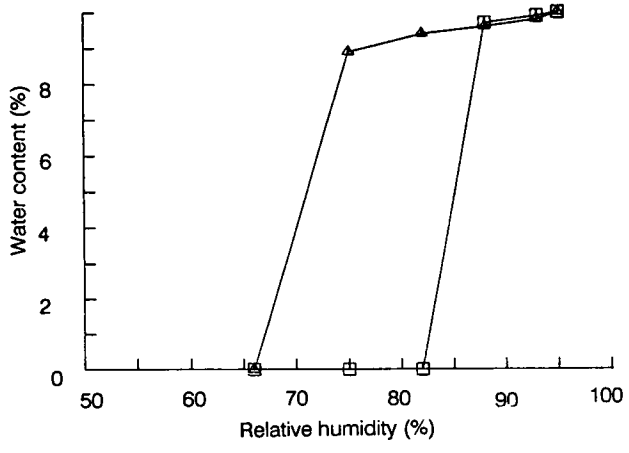

FIG. 6. Water content vs RH diagram of types I and II theophylline anhydrate. □, type I; △, type II.

Hydration kinetics of types I and II theophylline anhydrate

The absorption profiles of types I and II are uniquely different (as shown in Fig. 5) which suggests that the initial hydration rate of type II was much faster than the rate at the last stage, whereas for type I the hydration rate at the last stage was much faster than the initial rate. Criado et al (1978) listed the kinetic model equations for several proposed mechanisms believed to operate in solid-state chemical reactions (Table 3). The absorption data of type I at 88% RH and type II at 75% RH were fitted to the various models with the correlation coefficients shown also in Table 3.

Discussion

Characterization of types I and II theophylline anhydrate

The X-ray diffraction pattern (Fig. 1), IR spectra (Fig. 2), heats of fusion and melting points (Fig. 3) of types I and II were not significantly different, suggesting that type I had the same crystal structure and crystallinity as type II. On the other hand, the crystal orientation in tablets was studied by X-ray diffraction (Fukuoka et al 1987). The difference in X-ray diffraction intensities of types I and II (Table 1) were apparently caused by the crystal orientation in the (h00) planes of the columnar crystals of type I, suggesting differences of crystal habits between types I and II in which type I had the predominate face (100).

The results of specific surface area measurements by two different methods (Table 2) may be interpreted in the light of the information from the photomicrographs (Fig. 4). Since air does not filter through the blind cracks in a particle, the fine primary particles in the secondary particle cannot be measured by the air permeability method, but the secondary particle diameter can be measured. On the other hand, the results from the BET method are considered to be close to the

Table 3. Kinetic equations for the most common mechanisms of solid-state decomposition (Criado et al 1978) and correlation coefficients of plots of function g(x) against time t for the hydration of theophylline anhydrates.

Symbol	g(x)	Mechanism	Correlation coefficients	
			Type I at 88% RH	Type II at 75% RH
R1	x	Zero-order (Polany-Winger equation)	0·9801	0·9541
R2	$2(1-(1-x))^{1/2}$	Two-dimensional phase boundary	0·9562	0·9774
R3	$3(1-(1-x))^{1/3}$	Three-dimensional phase boundary	0·9366	0·9837
F1	$-\ln(1-x)$	First-order	0·8854	0·9933
A2	$(-\ln(1-x))^{1/2}$	Two-dimensional growth of nuclei[a]	0·9645	0·9643
A3	$(-\ln(1-x))^{1/3}$	Three-dimensional growth of nuclei[a]	0·9844	0·9469
D1	X^2	One-dimensional diffusion	0·9389	0·9887
D2	$(1-x)\ln(1-x)+x$	Two-dimensional diffusion	0·9009	0·9925
D3	$(1-(1-x)^{1/3})^2$	Three-dimensional diffusion[b]	0·8327	0·9921
D4	$(1-2x/3)-(1-x)^{2/3}$	Three-dimensional diffusion[c]	0·8783	0·9917

[a] Avrami equation; [b] Jander equation; [c] Ginstiling-Brounshtein equation.

true values, since nitrogen gas is adsorbed on the surfaces of the cracks. The results suggest that type I had the same crystalline structure as type II, but type II had large secondary particles containing very fine primary particles, while type I had small particles without defects. The results of gas affinity balance (Table 2) and comparison of the initial hydration rate of type I and type II (Fig. 5) suggest that the particle surface of type II was more hydrophilic than that of type I.

Hydration kinetics of types I and II theophylline anhydrate

Since the pattern of the absorption profile of type I (Fig. 6) was different from that of type II, it seems that the hydration mechanism of type I was different from that of type II. We attempted to fit the data to a number of proposed models (Table 3) but the high correlation coefficient in most curves precluded a definitive choice being made.

Acknowledgements

We thank Miss Hisako Saito for assistance with the experiments.

References

Criado, J. M., Morales, J., Rives, V. (1978) Computer kinetics analysis of simultaneously obtained TG and DTG curves. J. Therm. Anal. 14: 221–228

Fukuoka, E., Makita, M., Yamamura, S. (1987) Evaluation of crystallite orientation in tablets by X-ray diffraction methods. Chem. Pharm. Bull. 35: 1564–1570

Naqvi, A. A., Bhattacharyya, G. C. (1981) Crystal data for anhydrous theophylline. J. Appl. Crystal. 14: 464

Otsuka, M., Kaneniwa, N. (1988) The dehydration kinetics of theophylline monohydrate powder and tablet. Chem. Pharm. Bull. 36: 4914–4920

Shefter, E., Higuchi, T. (1963) Dissolution behavior of crystalline solvated and nonsolvated forms of some pharmaceuticals. J. Pharm. Sci. 52: 781–791

Shefter, E., Fung, H., Mok, O. (1973) Dehydration of crystalline theophylline monohydrate and ampicillin trihydrate. Ibid. 62: 791–794

Sutor, J. (1958) The structures of the pyrimidines and purines. VI. The crystal structure of theophylline. Acta Cryst. 11: 83–87